 doi:10.20944/preprints202204.0286.v1

Mechanical Property Analysis of Cuttlebone-like Structure under Compression and Shearing

Fan Wu[1] and Bo-Hua Sun[1]

[1] *School of Civil Engineering & Institute of Mechanics and Technology Xi'an University of Architecture and Technology, Xi'an 710055, China*
Corresponding author: email: sunbohua@xauat.edu.cn

The cuttlebone-like structure is a complex porous bionic structure with asymmetric sinusoidal S-shaped wall structure connecting laminar septa, and studies have shown that the cuttlebone-like structure has light weight, high strength and excellent energy absorption capability. It has become an important research to investigate the mechanical mechanism of cuttlebone-like structure and to design a bionic structure beyond nature structure based on it. In order to investigate the mechanical properties of the static compression and shearing processes of the cuttlebone-like structure, this paper establishes theoretical formulas and analyzes the influence of dimensionless parameters such as height-to-thickness ratio λ, period-to-thickness ratio ξ and amplitude to period ratio η on the compression and shearing processes with the help of ABAQUS finite element software.The parameter sensitivity analysis method was used to compare the important influence degree of each dimensionless parameter on the mechanical properties of the structure and to determine the relative optimal parameters of the structural mechanical properties under compression and shearing. Based on the relatively optimal parameter of the cuttlebone-like structure, the cross-sectional geometry of the structure is improved to build a new cuttlebone-like structure.The experimental results showed that the new cuttlebone-like structure with revised cross-section improved the mechanical properties of the cuttlebone-like structure.The study results are of theoretical guidance to enhance the mechanical properties and geometric design of cuttlebone-like structures.

Keywords: Cuttlebone-like structure; Bionic structure; Finite element analysis; 3D Printing; Compression; Shearing

I. INTRODUCTION

With billion years of natural evolutionary selection, each creature in nature has its own unique characteristics.Scholars have been inspired by various creatures in nature and have built bionic structures. Jiang et al[1] analyzed the microstructural characteristics of beetle sheath wings by observing the cross-sectional microstructure of beetle sheath wings and designed a porous structure formed by the crossover of transverse hollow tubes and longitudinal hollow tubes. Ma et al[2] investigated the microstructure of shell pearl layer and found that it is a multi-level "brick-mud" structure with alternating calcium carbonate and organic matter, which has the mechanical properties of high strength and high toughness. Meyers et al[3] investigated the beak structure of the toucan and found that this beak consists of a foam-like internal sandwich structure and an angular shell, which is similar to the traditional composite sandwich panel structure and has excellent characteristics of light weight and high strength. The bionic structures have excellent mechanical properties and 3D printing technology, also known as Additive Manufacturing, provides technical support to realize the manufacturing and processing of bionic structures[4–12], which make bionic structures have a wide range of research directions and application prospects in various fields such as aerospace, architecture, marine, and medical[13–19].

Scholars[20–23] have found that the internal structure of cuttlebone consists of parallel layers, and the interlayer core structure is a porous structure consisting of asymmetrically twisted S-shaped walls. It is due to this special structure that cuttlefish can resist large hydrostatic pressures in deep-sea environments(100-400m) and ensure their survival. Therefore, the structure of cuttlefish bone has been increasingly studied in depth. Mao et al[24] proposed a design of a cuttlebone structure based on the study of cuttlebone, and also developed a core structure similar to cuttlebone by 3D printing. The ex-

Preprints (www.preprints.org) | NOT PEER-REVIEWED | Posted: 29 April 2022 doi:10.20944/preprints202204.0286.v1

perimental results showed that the designed structure has the characteristics of light weight, high strength, and high energy absorption capacity. In summary, the cuttlebone-like structure based on the cuttlebone structure is a core structure with excellent mechanical properties.

In this paper, the theoretical analysis of the cuttlebone-like wall structure under compression and shearing is carried out by small deformation theory, and the variable parameter analysis of the cuttlebone-like structure under compression and shearing is carried out by using the finite element software ABAQUS. Inspired by the cuttlebone-like wall structure, this paper developed a new cuttlebone-like core structure by 3D printing, and analyzes the mechanical properties of the new cuttlebone-like core structure under compression and shearing with the help of finite element and experimental methods. The results of the study provide a reference for the theoretical study and structural design of cuttlebone-like structures.

II. MECHANICAL PROPERTY ANALYSIS OF CUTTLEBONE-LIKE STRUCTURE

A. Basic parameters

Mao et al. [24] used X-ray microcomputer(Micro-CT) scan tomography to obtain fully complex cuttlebone structures. In order to design simple structure, Mao et al. [24] simplified the structural characteristics of the cuttlebone structure to a sinusoidal S-shaped wall structure, and the designed dimensional parameters were proportional to the values of the natural cuttlebone structure. This paper delves into the influence of structural features and design parameters on the structure. The schematic diagram of the structure is shown in Figure 1 (the cross-sectional area and height of the wall structure remain unchanged to ensure that the total volume of the wall structure remains the same).

Referring to the numerical magnitude of the natural cuttlefish bone structure obtained from the study of Mao et al. [24], we set the parameter thickness $h = 0.33mm$, the period-to-thickness ratio $\xi = \frac{P}{h} = 9 \sim 18$, the height-to-thickness ratio $\lambda = \frac{L}{h} = 30 \sim 60$, the amplitude to period ratio$\eta = \frac{A}{P} = \frac{1}{15}, \frac{2}{15}, \frac{3}{15}, \frac{4}{15}, \frac{5}{15}$, density $\rho = 0.18\text{g/cm}^3$, modulus of elasticity $E = 1420\text{MPa}$ and Poisson's ratio $\nu = 0.3$ (as shown in Fig.1).

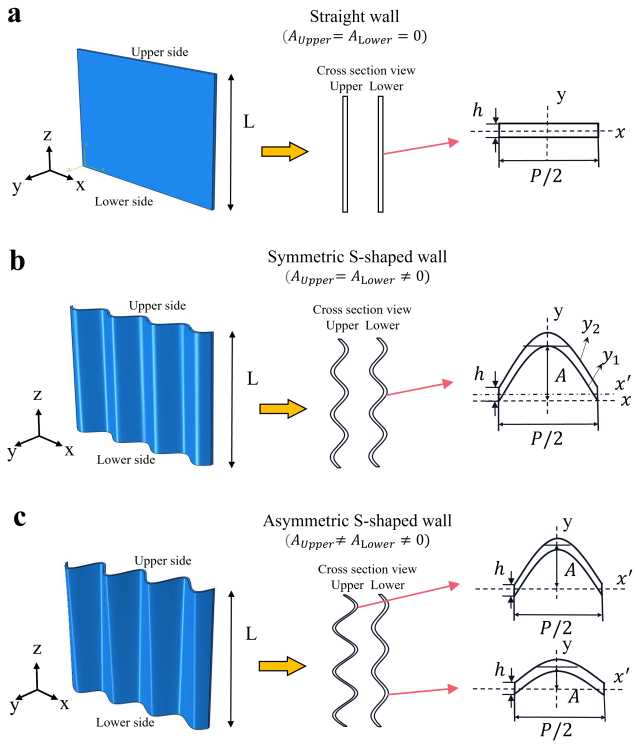

FIG. 1: Schematic diagram of structure and cross-section. a) Straight wall structure; b) Symmetrical S-wall structure; c) Asymmetric S-wall structure. P, A, h and L respectively represent period, amplitude, thickness and height.

To identify the different asymmetric S-shaped wall structures, they are named according to the ratio of amplitude to period between the top and bottom. For example, S4-S2 means $\eta_{upper} : \eta_{lower} = \frac{4}{15} : \frac{2}{15} = 4 : 2$ asymmetric S-shaped wall structure model, S2-S2 means $\eta_{upper} : \eta_{lower} = \frac{2}{15} : \frac{2}{15} = 2 : 2$ symmetric S-shaped wall structure model, and S0-S0 denotes the straight-wall structure model. The S3-S1,S3-S2,S4-S1,S4-S2,S4-S3,S5-S1,S5-S2 structures are cuttlebone-like structures.

Referring to the cross section of the straight wall structure in Fig.1a, the basic equation for establishing the moment of inertia of an area around the x-axis by taking a half-cycle is $I_x = \int_S y^2 dS$, where $dS = \frac{P}{2}dy$ is the differential region, x and y are the reference axes, and the y-axis is orthogonal to the x-axis. Therefore,

$$I_x = \int_{-\frac{h}{2}}^{\frac{h}{2}} \frac{P}{2} y^2 dy = \frac{Ph^3}{24}, \tag{1.1}$$

where P is the period of the sine curve and h is the thickness representing the perpendicular to the y direction.

Preprints (www.preprints.org) | NOT PEER-REVIEWED | Posted: 29 April 2022 doi:10.20944/preprints202204.0286.v1

Similarly, themoment of inertia of an area around the y-axis is

$$I_y = \int_{-\frac{P}{4}}^{\frac{P}{4}} hx^2 dx = \frac{hP^3}{96}. \tag{1.2}$$

Since the period P is much larger than the thickness h, $I_x \ll I_y$, the structure is prone to bending and buckling around the x-axis direction. When the number of periods is m, the moment of inertia of an area of the straight-walled structure is

$$I_0 = \frac{mPh^3}{12}. \tag{1.3}$$

Referring to the cross section of the symmetric S-shaped wall structure in Fig.1b, $y_1 = A \cdot cos\frac{2\pi}{P}x$, $y_2 = A \cdot cos\frac{2\pi}{P}x + n$, $dS = \frac{P}{\pi}(\arccos\frac{y-n}{A} - \arccos\frac{y}{A})dy$, establishing the equation for the half-cycle moment of inertia of an area around the x-axis as

$$\begin{aligned} I_x &= \int_S y^2 dS \\ &= \int_S \frac{P}{\pi} y^2 (\arccos\frac{y-h}{A} - \arccos\frac{y}{A})dy \\ &= \int_0^h \frac{P}{\pi} y^2 (h - \arccos\frac{y}{A})dy + \\ &+ \int_h^{A-h} (\frac{P}{\pi} y^2 \arccos\frac{y-h}{A} - \arccos\frac{y}{A})dy + \\ &+ \int_{A-h}^{A} (\frac{P}{\pi} y^2 \arccos\frac{y-h}{A} - A)dy \\ &= \frac{PhA^2}{4} + \frac{PAh^2}{\pi} + \frac{Ph^3}{16}. \end{aligned} \tag{1.4}$$

Similarly, the moment of inertia of an area around the y-axis is

$$I_y = \int_{-\frac{P}{4}}^{\frac{P}{4}} hx^2 dx = \frac{hP^3}{96}. \tag{1.5}$$

When the amplitude A is larger, I_x is larger than I_y, and the local structure is buckling around the y direction. When the amplitude A is small, I_x is lower than I_y, and the structure is easy to bend around the x-axis. When the number of periods is m, the moment of inertia of an area of the symmetric S-shaped wall structure is

$$I_x = mPhA^2 + \frac{4mPAh^2}{\pi} + \frac{mPh^3}{4}. \tag{1.6}$$

When the amplitude P of the wall structure takes 0, the symmetric S-shaped shaped wall structure degenerates to a straight wall structure, and its moment of inertia of an area becomes $\frac{mPn^3}{4}$. Since the moment of inertia of an area of the symmetric S-shaped wall structure is different from that of the straight wall structure around the axis, the coefficients of the equations for the moment of inertia of an area of the degraded symmetric S-shaped wall structure differ from those of the straight wall structure. Therefore, this paper increases the discount factor k_0 to obtain the equation of moment of inertia of an area of the symmetric structure around x' axis approximately as (k_0 is the discount factor)

$$I_0 = \frac{mPhA^2}{k_0} + \frac{4mPAh^2}{\pi k_0} + \frac{mPh^3}{12}. \tag{1.7}$$

B. Theoretical development and finite element analysis of structures under compression

In order to investigate the relationship between the compressive capacity and each parameter of S-shaped structures under compression. With the help of the Eulerian critical buckling equation mentioned by Mao et al. [24], a linear buckling theory model formulation for the cuttlebone-like structure was developed.

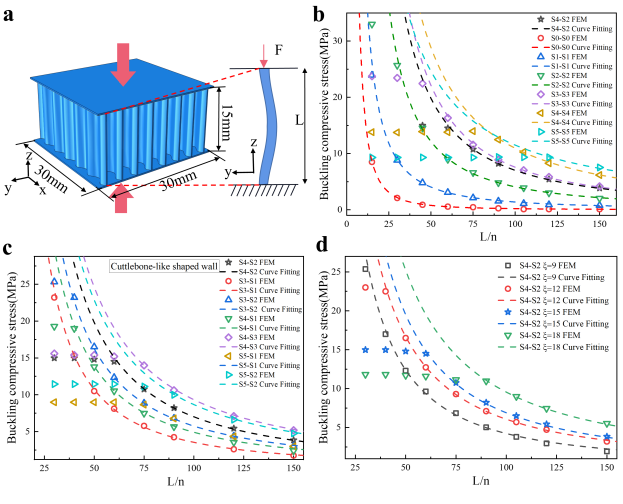

FIG. 2: Study of linear buckling of wall structures under compression. a) Schematic diagram of cuttlefish-like bone structure and buckling of wall structure under compression. b) Finite element and curve fitting of symmetric S-shaped wall structural buckling. c) Finite element and curve fitting of cuttlebone-like wall structural buckling. d) Finite element and curve fitting of the S4-S2 wall structural buckling for different values of ξ. ξ and λ respectively represent the period-to-thickness ratio and height-to-thickness ratio.

Preprints (www.preprints.org) | NOT PEER-REVIEWED | Posted: 29 April 2022 doi:10.20944/preprints202204.0286.v1

From the above, when the amplitude A is larger, $I_x \gg I_y$, the symmetric S-shaped structure is locally buckling around the y-axis direction. When the amplitude A is small, $I_x \ll I_y$, the symmetric S-shaped structure is bending and buckling around the x-axis direction as in Fig.2a.

The basic Eulerian critical buckling equation is established as

$$F_{bulking} = \frac{\pi^2 E I_0}{kL^2}. \tag{2.1}$$

Eq.(1.7) is substituted into Eq.(2.1)

$$\begin{aligned}\sigma_{bulking} &= \frac{F_{bulking}}{B} = \frac{\pi^2 E m I_0}{kL^2 B} = \frac{\pi^2 E}{k\frac{L^2 B}{mI_0}} \\ &= \frac{\pi^2 E}{k\frac{L^2 mnP}{\frac{mPhA^2}{k_0}+\frac{4mPAh^2}{\pi k_0}+\frac{mPh^3}{12}}} \\ &= \frac{\pi^2 E(\frac{1}{k_0}\frac{A^2}{h^2}+\frac{4}{\pi k_0}\frac{A}{h}+\frac{1}{12})}{k\frac{L^2}{h^2}},\end{aligned} \tag{2.2}$$

where $F_{bulking}$ is the critical buckling load; $\sigma_{bulking}$ is the critical buckling compressive stress; E is the material modulus of elasticity; I_0 is the moment of inertia of an area(which depends on the geometry of the section); k is the correction factor; B is the area of the section($B = m \cdot h \cdot P$); and m is a positive integer.

Considering the effect of the period P of the x-axis on the critical buckling stress, Eq.(2.2) is changed to Eq.(2.3)

$$\sigma_{bulking} = \frac{\pi^2 E(\frac{1}{k_0}\frac{P^2}{h^2}\frac{A^2}{P^2}+\frac{4}{\pi k_0}\frac{P}{h}\frac{A}{P}+\frac{1}{12})}{k\frac{L^2}{h^2}}. \tag{2.3}$$

Since the height-thickness ratio $\frac{L}{n} = \lambda$, the period-thickness ratio $\frac{P}{n} = \xi$, the amplitude to period ratio $\frac{A}{n} = \eta$, and the correction factor $\frac{k}{k_0} = k_1$, the substitution into Eq.(2.3) yields

$$\sigma_{bulking} = \frac{\pi^2 E\xi^2\eta^2}{k_1\lambda^2} + \frac{4\pi E\xi\eta}{k_1\lambda^2} + \frac{\pi^2 E}{12k_0\lambda^2}. \tag{2.4}$$

Considering the asymmetric S-shaped structure, simplifying the first two terms of Eq.(2.4) and distinguishing the parameters of the upper and lower section η values, the result is

$$\sigma_{bulking} = \frac{\pi^2 E\xi^2(\eta_{upper}^2+\eta_{lower}^2)}{2k_2\lambda^c} + \frac{\pi^2 E}{12k_0\lambda^2}. \tag{2.5}$$

where k_2 is the correction factor, c is a real number, η_{upper} is the upper amplitude period ratio, and η_{lower} is the lower amplitude period ratio.

To verify the reasonableness of the formula, the linear buckling results of the simulated wall structure in ABAQUS were compared with the theoretical curves. As shown in Fig.2b,c,d, the results basically match. Comparing Fig.2b,c, it is found that the cuttlefish-like bone wall structure has a better compression resistance compared to other wall structures. Observing Fig.2c,d, it is found that when the height-thickness ratio λ is greater than 60, the wall structure is in integral buckling and the buckling compressive stress is inversely proportional to the λ, proportional to the η of the upper and lower section($\eta_{upper/lower}$) and ξ; when λ is less than 60, the wall structure exhibits local buckling for larger buckling stresses, but no longer satisfies the theoretical equation. The above results verified that the amplitude to period ratio $\eta_{upper/lower}$ of S3-S1,S3-S2,S4-S1,S4-S2,S4-S3,S5-S1,S5-S2 structures, the height-thickness ratio λ of $30 \sim 60$, and the period-thickness ratio ξ of $9 \sim 18$ can increase the bending stiffness of the wall structure and improve the overall structural compressive capacity.

To further analyze the effect of different parameters on the compressive capacity of the structure, the three-dimensional compression model (size $30mm \times 30mm \times 15mm$) was established as in Fig.2a and the mechanical properties of the structure were analyzed by Abaqus software. Fig.3a compares the curves of the simulated and experimental[24] results for the S0-S0, S2-S2, and S4-S2 structures of $\xi = 15$ and $\lambda = 45$, and Figure 3b,c respectively show the specific compressive strength of the structures of $\xi = 15$ and $\lambda = 45$ at different $\eta_{upper/lower}$ under finite element and experimental[24]. The comparison of finite element and experimental results are basically consistent, which verifies the accuracy of the finite element results. Fig.3d shows the magnitude of the compressive strain energy of the structure of $\xi = 15$ and $\lambda = 45$ at different $\eta_{upper/lower}$ values. Combined with Fig.3c,d, it is found that the S4-S2 structure in the cuttlebone-like structure has a large compressive strength and energy absorption capacity at the same time. Therefore, Fig.3e,f provides a more in-depth analysis of the effects of different ξ and λ on the compressive strength and strain energy of the S4-S2 structure. As in Fig.3e, the compressive strength of S4-S2 structure decreases continuously as λ increases, and the S4-S2 structure has the maximum strain energy at $\lambda = 45$. As shown in Fig.3f, the S4-S2 structure has the maximum compressive strength at

Preprints (www.preprints.org) | NOT PEER-REVIEWED | Posted: 29 April 2022 doi:10.20944/preprints202204.0286.v1

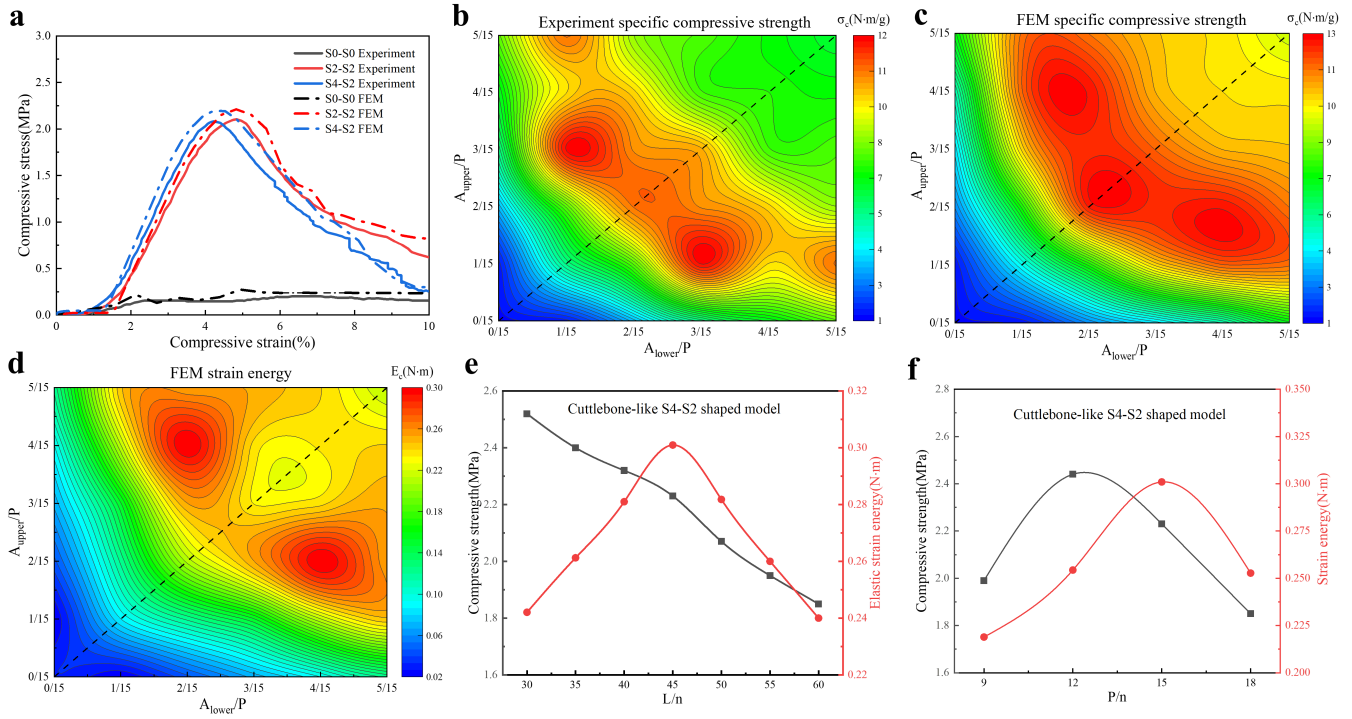

FIG. 3: Study of the mechanical properties of structures under compression. a) Compressive stress-strain curves for the three models S0-S0,S2-S2,S4-S2. b,c) Compressive strength of various symmetric S-shaped and asymmetric S-shaped structural models under finite element and experimental[24]. d) Compressive strain energy of various symmetric S-shaped and asymmetric S-shaped structural models under finite elements. e,f) Compressive strength and strain energy of S4-S2 model with different ξ and λ values under finite elements. h, A, P, σ_c, and E_c respectively represent the thickness, amplitude, period, specific compressive strength, and compressive strain energy.

$\xi = 12$ and the S4-S2 structure has the maximum strain energy at $\xi = 15$.

Combining the formula with the finite element, the analysis results show that increasing the $\eta_{upper/lower}$ and ξ will increase the bending stiffness of the wall structure and make the wall structure change from overall buckling around the x direction to local buckling around the y direction; when the $\eta_{upper/lower}$ and ξ is too small, the wall structure degenerates into a straight wall structure with less bending stiffness and the bearing capacity decreases; when the $\eta_{upper/lower}$ and ξ is too large, the corrugated local thickness of the wall structure is too thin to buckle and the bearing capacity decreases. The analysis results also show that as $\eta_{upper/lower}$ increases, it will reduce the bending stiffness of the wall structure; when $\eta_{upper/lower}$ is too small, the bending stiffness of the wall structure will be too large, be prone to material damage, and decrease the load-bearing capacity of the structure; when $\eta_{upper/lower}$ is too large, the bending stiffness of the wall structure will be too small, be prone to structural damage, and decrease the load-bearing capacity of the structure. In summary, the effects of different parameters on the structure were analyzed under compression. For further analysis, we will further analyze the shearing properties of the structure.

C. Theoretical development and finite element analysis of structures under shearing

In addition to the excellent compression resistance, the excellent shearing resistance of the cuttlebone-like structure is also an important feature. The following section will mainly study the relationship between the shearing strength and each parameter of the cuttlebone-like structure under shearing. Firstly, a schematic diagram of structural shearing is established as Fig.4a.

Preprints (www.preprints.org) | NOT PEER-REVIEWED | Posted: 29 April 2022 doi:10.20944/preprints202204.0286.v1

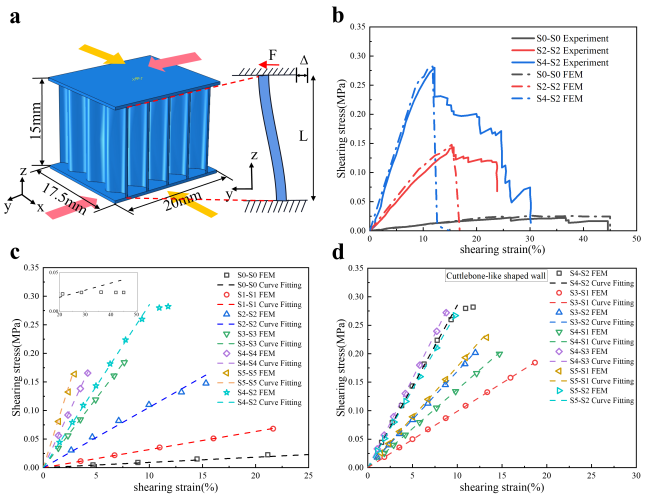

FIG. 4: Linear deformation analysis of wall structures under shear loading along the y-axis. a) Schematic diagram of shearing of cuttlefish-like bone structure and shearing deformation of wall structure along y direction. b) Finite element's and experimental[24] shear stress-strain curves for three models of S0-S0,S2-S2,S4-S2 under shearing along the y-axis direction. c,d) Finite element and theoretical curve fitting of linear deformation of symmetric S-shaped wall structure and cuttlebone-like wall structure under shearing along the y-axis direction.

To analyze the shearing deformation of the structure along the y-direction, the shearing deformation equation is established with reference to the principle of D'Alembert principle[25] as

$$F = K \cdot \Delta = \frac{EI_0}{kL^3}\Delta. \tag{2.6}$$

Substituting Eq.(1.7) into Eq.(2.6) yields

$$\begin{aligned}\tau = \frac{F}{B} &= \frac{EmI_0}{kL^2B}\frac{\Delta}{L} = \frac{E}{k\frac{L^2B}{mI_0}}\varepsilon \\ &= \frac{E}{k\frac{L^2mhP}{m(\frac{1}{k_0}hPA^2+\frac{4}{\pi k_0}h^2PA+\frac{1}{12}h^3P)}}\varepsilon \\ &= \frac{E(\frac{1}{k_0}\frac{P^2}{h^2}\frac{A^2}{P^2}+\frac{4}{\pi k_0}\frac{P}{h}\frac{A}{P}+\frac{1}{12})}{k\frac{L^2}{h^2}}\varepsilon\end{aligned} \tag{2.7}$$

Since the height-thickness ratio $\frac{L}{n} = \lambda$, the period-thickness ratio $\frac{P}{n} = \xi$, the amplitude to period ratio $\frac{A}{n} = \eta$, and the correction factor $\frac{k}{k_0} = k_1$, the substitution into Eq.(2.7) yields

$$\tau = (\frac{\xi^2}{k_1}\eta^2 + \frac{4\xi}{\pi k_1}\eta + \frac{1}{12k_0})\frac{E\varepsilon}{\lambda^2}, \tag{2.8}$$

where F is the shearing load; τ is the shearing stress; K is the stiffness; Δ is the shearing displacement; ε is the shearing strain; E is the modulus of elasticity; I_0 is the moment of inertia of an area(which depends on the geometry of the cross-section); k is the correction factor; B is the cross-sectional area; L is the plate height($B = m \cdot h \cdot P$); and m is a positive integer.

Considering the asymmetric S-shaped structure, simplifying the first two terms of Eq.(2.8) and distinguishing the parameters of the η of upper and lower section, the result is

$$\tau = \frac{E\xi^2(\eta_{upper}^2 + \eta_{lower}^2)}{2k_2\lambda^2}\varepsilon, \tag{2.9}$$

where k_2 is the correction factor, η_{upper} is the upper amplitude to period ratio, and η_{lower} is the lower amplitude to period ratio.

A three-dimensional shearing model (size $20mm \times 17.5mm \times 15mm$) is created as in Fig.4a. Fig.4b compares the finite element and experimental[24] curves of S0CS0, S2CS2 and S4CS2 models under the shearing along the y-axis direction. The results show that the linear stage of the structure before shearing failure is basically consistent(the simulation object is an ideal shear model, so the structure loses the shearing bearing capacity after failure, but the uneven material in the experiment leads to a certain bearing capacity after failure), which verifies the accuracy of the finite element results. As shown in Fig.4c,d, the simulation results of the structure in the linear shearing deformation stage basically meet the theoretical formula, and it is found that the cuttlebone-like structure has better shearing resistance than other structures. In order to analyze the influence of different parameters on the mechanical properties of the structure, Fig.5a,b are the specific shearing strength and shearing strain energy of the structure of $\xi = 15$ and $\lambda = 45$ under different $\eta_{upper/lower}$ by the finite element. It is found that the S4-S2 structure in the cuttlebone-like structure has large shearing strength and energy absorption ability. For further analysis, Fig.5c,d considers the influence of different ξ and λ on the shearing strength and shearing strain energy of S4-S2 structure. As shown in Fig.5c, the shearing strength of S4-S2 structure decreases with the increase of λ, but the shearing strain energy increases. As shown in Fig.5d, the shearing strength of S4-S2 structure increases with the increase of ξ, and the shearing strain energy is the largest in $\xi = 12$. Combined with

Preprints (www.preprints.org) | NOT PEER-REVIEWED | Posted: 29 April 2022 doi:10.20944/preprints202204.0286.v1

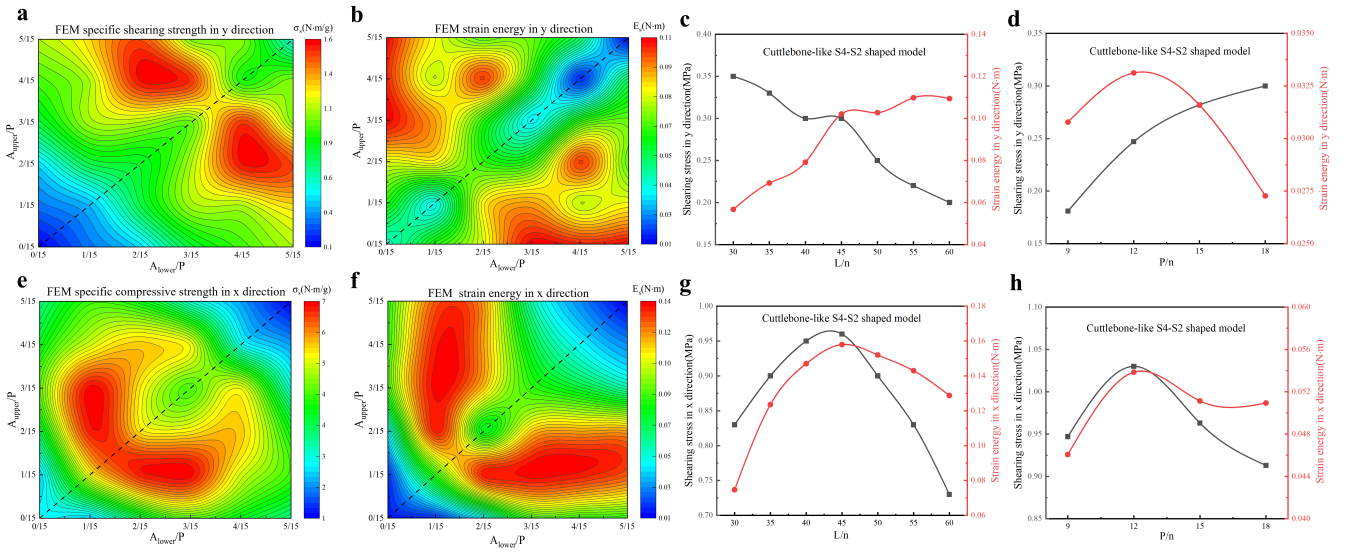

FIG. 5: Study of the mechanical properties of structures under shearing. a,e) Shearing strength along the y and x-axis for various symmetric S-shaped and asymmetric S-shaped structural models under finite elements. b,f) Shearing strain energy along the y and x-axis for various symmetric S-shaped and asymmetric S-shaped structural models under finite elements. c,g) Shearing strength and strain energy along the y and x-axis for S4-S2 structural models with different λ in finite elements. d,g) Shearing strength and strain energy along the y and x-axis for S4-S2 structural models with different ξ in finite elements. h, A, P, σ_s, and E_s respectively represent thickness, amplitude, period, specific shearing strength, and shearing strain energy.

the theoretical formula and finite element method, the results show that increasing the $\eta_{upper/lower}$ and ξ can increase the shearing stiffness of the structure and improve the shearing capacity of the structure. When the $\eta_{upper/lower}$ and ξ are too small, the shearing stiffness of the structure is insufficient, and the shearing capacity of the structure decreases; When the $\eta_{upper/lower}$ and ξ are too large, the structure and the connection surface are prone to material damage, resulting in a decrease in the shearing capacity of the structure. The results still express that the increase of λ will reduce the shearng stiffness of the structure and weaken the shearing capacity of the structure; when λ is too small, the shearing stiffness of the structure is too large, the structure is prone to material shearing failure, and the shearing capacity of the structure decreases; when λ is too large, the shearing stiffness of the structure is insufficient, and the shearing capacity of the structure decreases.

In addition to the shearing analysis of the structure along the y-axis direction, the shearing capacity of the structure under shearing along the x-axis direction is also studied. According to the specific shearing strength and shearing strain energy of the structure with different $\eta_{upper/lower}$ by the finite element in Fig.5e,f, it is found that the cuttlebone-like structure of S3-S1, S3-S2, S4-S1, S4-S2 types have relatively excellent specific shearing strength and shearing strain energy. Combined with the above, the S4-S2 structure is selected as the invariant to further analyze the influence of ξ and λ on the shearing capacity of the structure along the x direction. As shown in Fig.5g,h, the S4-S2 structure has the maximum shearing strength and shearing strain energy at $\lambda = 45$ and $\xi = 12$. Combined with the research[26] and the finite element results, when the $\eta_{upper/lower}$ and ξ are large, the stiffness of the section along the x direction decreases and the shearing capacity is weak; when the $\eta_{upper/lower}$ and ξ are too small, the structure and the connection surface are prone to material damage, and the shearing capacity is weak; when the λ value is large, the shearing capacity of the cross section along the x direction is weak; when the λ value is too small, the structure and the connection surface are prone to material damage and the shearing capacity is weak.

Preprints (www.preprints.org) | NOT PEER-REVIEWED | Posted: 29 April 2022 doi:10.20944/preprints202204.0286.v1

III. DESIGN AND ANALYSIS OF NEW CUTTLEBONE-LIKE STRUCTURES

Based on the above analysis, when ξ is 15 and λ is 45, the S4-S2 structure has relatively excellent mechanical properties. Therefore, on the basis of S4-S2 structure, the new cuttlebone-like structure is improved, and the mechanical properties are analyzed by finite element method as shown in Fig.6.

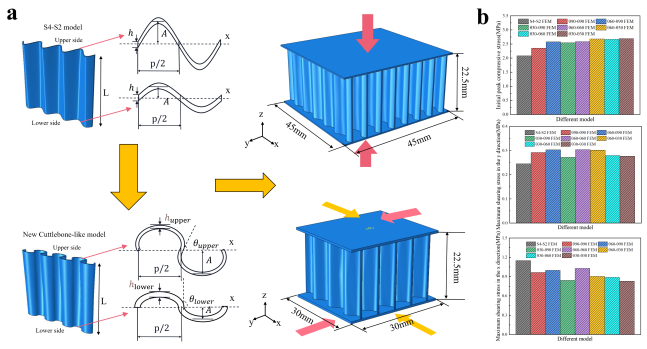

FIG. 6: Design and finite element analysis of new cuttlebone-like structures. a) S4-S2 type wall structure and new cuttlebone-like wall structures schematic diagram under compression and shearing. b) Comparison of compressive and shearing strength between S4-S2 structure and new cuttlebone-like structures under finite element. h, A, P, θ and L respectively represent thickness, amplitude, period, angle and height.

It can be seen from the above that structures increases the stiffness by increasing the section modulus, so as to improve the compressive and shearing resistance of the structure. The section is improved to elliptic(where the θ value can change the shape of the ellipse) as shown in Fig.6. In order to ensure that the improved structure has the same volume and section area as the original structure, the section thickness is $h_{upper/lower} = \frac{B}{s} = \frac{mhP}{s}$ (s represents the arc length of the ellipse center line[27, 28]). S4-S2 structure takes thickness $h = 0.5mm$, upper section amplitude $A_{upper} = 2$, lower section amplitude $A_{lower} = 1$, period $P = 7.5mm$, height $L = 22.5mm$. New cuttlebone-like structures takes section upper angle $\theta_{upper} = 90, 60, 30$, lower section angle $\theta_{lower} = 90, 60, 30$, upper section thickness $h_{upper} = 0.3, 0.28, 0.24mm$, and lower section thickness $h_{lower} = 0.4, 0.38, 0.34mm$. The parameters of new cuttlebone-like structures are the same as those of S4-S2 structure. The three-dimensional compression model(size $45mm \times 45mm \times 22.5mm$) and three-dimensional shearing model(size $25mm \times 25mm \times 22.5mm$) were established, and the mechanical properties of the structure were analyzed by finite element method as shown in Fig.6b. In order to facilitate the identification of different new structures, it is named according to the angle between the upper and lower section. For example, θ90-θ90 represents a model of $\theta_{upper} = 90$ and $\theta_{lower} = 90$ structure. It is found in Fig.6b that the compressive strength and shearing capacity along the y direction of new cuttlebone-like structures are greatly improved compared with those of the S4-S2 structure. Although the shearing capacity along the x direction will decrease, it is still 2 to 3 times larger than that in the y direction.

In order to further study the mechanical properties of the new cuttlebone-like structure under compression and shearing, the experimental model was obtained by SLA880 3D printer and the compression and shearing experiment were completed by MTS electronic universal testing machine. The experimental material used C-UV9400E photosensitive resin, material density $\rho = 1.15\text{g/cm}^3$, elastic modulus $E = 2700\text{MPa}$, Poisson's ratio $\nu = 0.3$. It is found that the θ_{lower} of the structure has little effect on the overall structural deformation and the θ_{upper} end will have a great influence on the structural deformation. Therefore, this paper selects S4-S2, θ90-θ90, θ60-θ90, θ60-θ90 as the deformation diagram of the experimental comparison, as shown in Fig.7. Fig.7a shows the compression experimental results. Both S4-S2 and θ90-θ90 structures show local buckling at the upper section. θ60-θ90 structure shows global buckling similar to shearing deformation, and θ30-θ90 structure shows global bending buckling. It can be seen from the stress-strain curves that the compressive capacity of the structures decreases continuously after buckling, and θ60-θ90 and θ60-θ60 structures have more excellent compressive capacity than the S4-S2. Fig.7b shows the shearing experimental results in the y direction. The deformation stage consists of three stages from material deformation to failure stage, of which θ60-θ90, θ60-θ60, θ30-θ90 and θ30-θ30 have better shearing capacity along y direction than S4-S2 structure. Fig.7c shows the shearing experimental results in the x direction. The S4-S2 structure is characterized by the overall fracture failure of the material at the section of the larger amplitude, and the θ90-

Preprints (www.preprints.org) | NOT PEER-REVIEWED | Posted: 29 April 2022 doi:10.20944/preprints202204.0286.v1

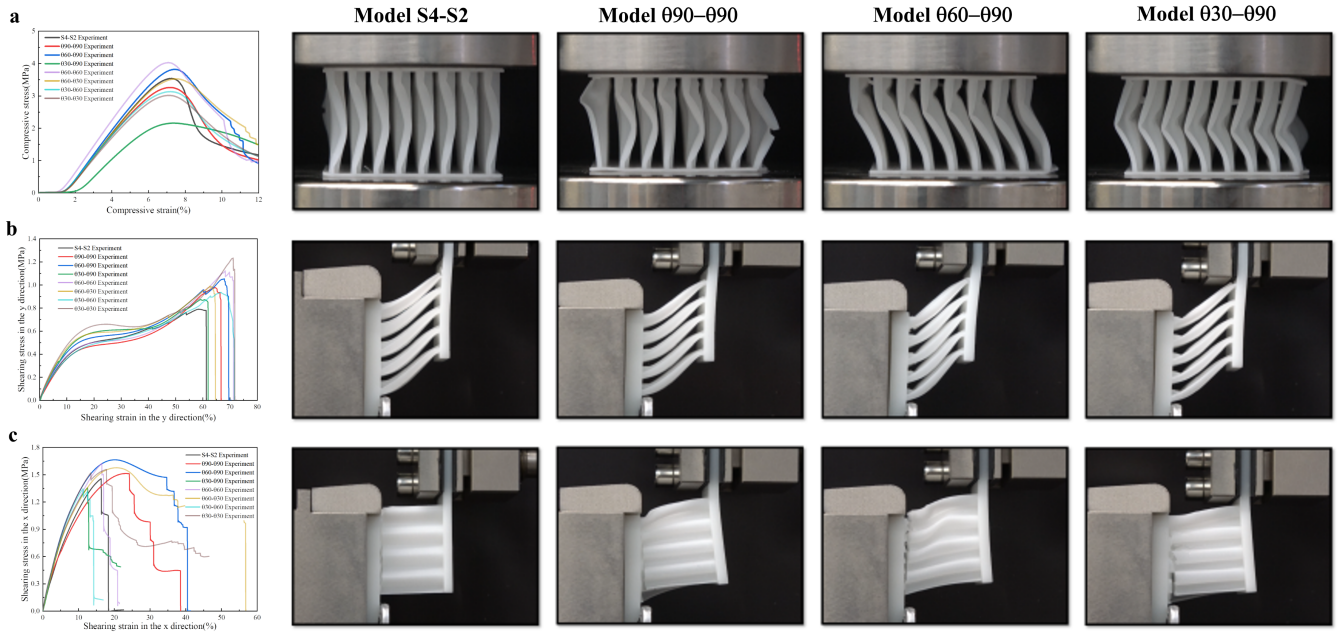

FIG. 7: Analysis of mechanical properties of new cuttlebone-like structures under experiment. a) The compressive stress-strain curves and experimental results of S4-S2 structure and new cuttlebone-like structures under compression. b) The shearing stress-strain curves and experimental results of S4-S2 structure and new cuttlebone-like structures under shearing along y-axis. c) The shearing stress-strain curves and experimental results of S4-S2 structure and new cuttlebone-like structures under shearing along x-axis.

θ90, θ60-θ90 and θ30-θ90 structures are characterized by shearing buckling to the fracture failure of the material at the section of the larger amplitude. It can be seen from the stress-strain curves that the material fracture failure of the structure after reaching a certain deformation, and θ60-θ90, θ60-θ60 and θ60-θ30 structures have more excellent shearing capacity along the x direction than the S4-S2. Based on the experimental results under compression and shearing, the proposed new θ60-θ90 structure has better compression and shearing resistance than all structures, and its compressive stress, shearing stress along y direction and shearing stress along x direction are respectively increased by 7.9%, 32.8% and 14.9% than S4-S2 structure.

IV. DISCUSSIONS AND CONCLUSIONS

In this paper, the numerical simulation method is used to study the mechanical properties of the compression and shearing process of the cuttlebone-like structure. Combined with the theoretical formula and the numerical simulation results, the mechanical mechanism is analyzed by parameter sensitivity analysis method, and the influence of geometric parameters on the mechanical properties is analyzed. Combined with the research results, designed new cuttlebone-like structures were verified by finite element and experiment, and the following conclusions were obtained :

(1)The effects of dimensionless parameters such as amplitude-period ratio, period-thickness ratio and height-thickness ratio on structural mechanical properties are analyzed theoretically. The rationality of the theoretical model and the parameter range of the structure is preliminarily verified, which provides a theoretical basis for the analysis of the cuttlebone-like structure;

(2)This paper analyzes the mechanical properties of the structure under different amplitude to period ratio, period to thickness ratio and height to thickness ratio by finite element method. The research results verify that the cuttlebone-like structure can ensure the effective compression and shearing stiffness and significantly improve the compression and shear resistance of the structure relative to the straight wall structure and symmetric S-shaped wall structure. It was determined that

 doi:10.20944/preprints202204.0286.v1

the S4-S2 structure of the cuttlefish-like bone structure with *xi* as 15 and *lambda* as 45 has relatively excellent mechanical properties;

(3)The analysis results show that the mechanical properties of some new types of cuttlebone-like structures under static compression and shearing are better than those of the S4-S2 shaped cuttlebone-like structure. The mechanical properties of the new θ60-θ90 structure were absolutely improved compared with those of the S4-S2 shaped cuttlebone-like structure, in which the compressive stress, shear stress in y direction and shear stress in x direction were respectively increased by 7.9%, 32.8% and 14.9%;

(4)The research results provide a reference for the improvement of the mechanical property and the geometric configuration design of the cuttlebone-like structure. However, further research is still needed for the expansion and application of the cuttlebone-like wall structure, and more in-depth exploration is still needed for the multi-layer structural mechanics principle of the cuttlebone-like structure.

ACKNOWLEDGMENTS

This work was supported by Xi'an University of Architecture and Technology (Grant No. 002/2040221134).

Conflict of interest The author declares that he has no known competing financial interests or personal relationships that could have appeared to influence the work reported in this paper.

Data availability The data that support the findings of this study are available from the corresponding author upon reasonable request.

[1] Zhixian Y. Research on microstructures, mechanical properties and coupling mechanism of beetle elytra [D]. NanJing: Nanjing University of Aeronautics and Astronautics, 2009.

[2] MA X Y, LIANG H Y, WANG L F. Multi-materials 3D printing application of shell biomimetic structure. Chinese Science Bulletin, 2015, 61(7): 728-734.

[3] Meyers M A, McKittrick J, Chen P Y. Structural biological materials: critical mechanics-materials connections. science, 2013, 339(6121): 773-779.

[4] Xuan L, Hong M, Shuangshuang L, et al. Research progress on 3D printing technology process control problem. Acta Automatica Sinica, 2016, 42(7): 983-1003.

[5] LI ZQ X L. Review of study on advanced light alloy materials and forming technique in spaceflight industry. Aerospace Shanghai, 2019, 36(2): 9-21.

[6] Espera A H, Dizon J R C, Chen Q, et al. 3D-printing and advanced manufacturing for electronics. Progress in Additive Manufacturing, 2019, 4(3): 245-267.

[7] Liu W, Liu T, Liao W, et al. Study and application of selective laser sintering/melting technology of ceramic materials. Bulletin of the Chinese Ceramic Society, 2014, 33(11): 2881-2896.

[8] Lin X, Huang W D. High performance metal additive manufacturing technology applied in aviation field. Materials China, 2015, 34(9): 684-688.

[9] Kan W, Lin J. Research progress on fabrication of TiAl alloys fabricated by additive manufacturing. Mat. China, 2015, 34: 111-119.

[10] Rahim T N A T, Abdullah A M, Md Akil H. Recent developments in fused deposition modeling-based 3D printing of polymers and their composites[J]. Polymer Reviews, 2019, 59(4): 589-624.

[11] Yang Y H. Analysis of classifications and characteristics of additive manufacturing (3D print). Advances in Aeronautical Science and Engineering, 2019, 10(3): 309-318.

[12] Acquah S F A, Leonhardt B E, Nowotarski M S, et al. Carbon nanotubes and graphene as additives in 3D printing. Carbon nanotubes-current progress of their polymer composites, 2016: 227-251.

[13] Eder M, Amini S, Fratzl P. Biological compositescomplex structures for functional diversity. Science, 2018, 362(6414): 543-547.

[14] Meyers M A, McKittrick J, Chen P Y. Structural biological materials: critical mechanics-materials connections. science, 2013, 339(6121): 773-779.

[15] Ji B, Gao H. Mechanical properties of nanostructure of biological materials. Journal of the Mechanics and Physics of Solids, 2004, 52(9): 1963-1990.

[16] Rivera J, Hosseini M S, Restrepo D, et al. Toughening mechanisms of the elytra of the diabolical ironclad beetle. Nature, 2020, 586(7830): 543-548.

[17] Zhang X, Xie J, Chen J, et al. The beetle elytron plate: a lightweight, high-strength and buffering functional-structural bionic material. Scientific Reports, 2017, 7(1): 1-7.

 doi:10.20944/preprints202204.0286.v1

[18] Yang X, Ma J, Shi Y, et al. Crashworthiness investigation of the bio-inspired bi-directionally corrugated core sandwich panel under quasi-static crushing load[J]. Materials a Design, 2017, 135: 275-290.

[19] XIONG J, Yuntong D U, Wen Y. Research progress on design and mechanical properties of lightweight composite sandwich structures. Journal of Astronautics, 2020, 41(6): 749-760.

[20] Birchall J D, Thomas N L. On the architecture and function of cuttlefish bone. Journal of Materials Science, 1983, 18(7): 2081-2086.

[21] Knöller A, Runčevski T, Dinnebier R E, et al. . Cuttlebone-like V2O5 nanofibre scaffoldsCadvances in structuring cellular solids. Scientific reports, 2017, 7(1): 1-8.

[22] Cadman J, Zhou S, Chen Y, et al. Cuttlebone: characterisation, application and development of biomimetic materials. Journal of Bionic Engineering, 2012, 9(3): 367-376.

[23] Yang T, Jia Z, Chen H, et al. Mechanical design of the highly porous cuttlebone: A bioceramic hard buoyancy tank for cuttlefish. Proceedings of the National Academy of Sciences, 2020, 117(38): 23450-23459.

[24] Mao A, Zhao N, Liang Y, et al. Mechanically efficient cellular materials inspired by cuttlebone. Advanced Materials, 2021, 33(15): 2007348.

[25] Pizhong Q, Sixin H, Zhimin L I, et al. Advances in Stability Analysis of Thin-Walled Curved Beams. Chinese Quarterly of Mechanics, 2020, 41(3): 385.

[26] Dou C, Pi Y L, Gao W. Shear resistance and post-buckling behavior of corrugated panels in steel plate shear walls. Thin-Walled Structures, 2018, 131: 816-826.

[27] Guo J C, Zhang Q G, Zhang L Z, et al. . Transformation formulas for the elliptic arc length and its application based on the elliptic integral of the second kind[J]. Mathematics in Practice and Theory, 2011, 41(24): 210-216.

[28] JIN J, ZHENG G, REN D, et al. Improved algorithm for arc length of sectional ellipse in geodetic problem. Science of Surveying and Mapping, 2015.